Observational Evidence for the Mutual Regulation of the Tropical Hydrological Cycle and Tropical Sea Surface Temperatures

GRAEME L. STEPHENS

Department of Atmospheric Science, Colorado State University, Fort Collins, Colorado

PETER J. WEBSTER

School of Earth and Atmospheric Sciences, and School of Civil and Environmental Engineering, Georgia Institute of Technology, Atlanta, Georgia

RICHARD H. JOHNSON

Department of Atmospheric Science, Colorado State University, Fort Collins, Colorado

RICHARD ENGELEN

European Centre for Medium-Range Forecasts, Bracknell, Berkshire, United Kingdom

TRISTAN L'ECUYER

Department of Atmospheric Science, Colorado State University, Fort Collins, Colorado

(Manuscript received 3 July 2003, in final form 5 January 2004)

ABSTRACT

From the analysis of surface, upper-air, and satellite observations it is suggested that the hydrological cycle associated with the Madden–Julian oscillation acts in the mode of a self-regulating oscillator. The regulation occurs as a feedback between hydrological processes in the atmosphere; radiation processes; and the dynamical movement of air over the tropical oceans controling variations of rainfall, cloudiness, and sea surface temperature (SST) on time scales varying between 30 and 60 days. The conjectured feedback occurs in three main phases: (i) the destablization phase: the atmosphere becomes increasingly unstable by the combination of radiative cooling of the upper troposphere, the gradual build up of shallow convection, and the warming of the SSTs under near-clear-sky and calm conditions; (ii) the convective stage: large-scale convection develops over the region resulting in widespread heavy precipitation, deepening of the oceanic mixed layer, cooling of the SST, and moistening of the upper troposphere; and (iii) the restoring phase: the combination of continued cooling of the SSTs maintained by the strong low-level winds and reduced solar heating, with the radiative heating of the upper atmosphere by high clouds sustained by high humidity, are major factors in stabilizing the atmosphere, suppressing convection, bringing an end to the cooling of the SSTs, and eventually leading to a calming of the winds, dissipation of the thick upper-level clouds, and a restoration of the cycle to its warming phase.

1. Introduction

The supply of freshwater upon which life on the planet depends is governed by a combination of complex physical processes that establish a cycle of water from the surface to the atmosphere and back to the surface, referred to as the hydrological cycle. Changes in this cycle through shifts in the amount and distribution of evaporation, clouds, and precipitation are critical to the functioning of the entire ecosystem. The variability of the hydrology cycle is complex, and managing changes that occur either by natural or by anthropogenic causes is perhaps the most important challenge confronting human society in the global change arena. The 1995 Intergovernmental Panel on Climate Change (IPCC) report (Houghton et al. 1995) speculates that ''warmer temperatures will lead to a more vigorous hydrological cycle; this translates into prospects of more severe droughts and/or floods in some places.'' However, to predict whether the hydrological cycle becomes invigorated or not under global warming requires an understanding of the processes that affect the hydrological

Corresponding author address: Dr. Graeme L. Stephens, Department of Atmospheric Science, Colorado State University, Fort Collins, CO 80523.
E-mail: stephens@atmos.colostate.edu

cycle and all relevant feedback mechanisms that alter its response to external climate forcings. These feedbacks, in one way or another, involve clouds and processes that affect clouds. At this stage, our understanding of these cloud-related feedbacks is unfortunately rudimentary and widely considered to be one of the major obstacles in the prediction of climate variability and climate change (Stephens et al. 2002).

Regions on the earth where feedbacks related to the hydrological cycle are both vigorous and of global consequence are the warm pool regions of the tropical oceans (Webster 1994). Moist air converges into these regions driven by both the east–west circulation of air along the equator and the trade winds that converge air from the midlatitudes toward the equator. This convergence supports development of convection that forms the deepest clouds, the heaviest rainfall, and largest release of latent heat on the planet. This convection undergoes distinct variability on all scales from the interannual time scales associated with the El Niño–Southern Oscillation (ENSO; e.g., Lau et al. 1989), as well as variability on time scales of 30–60 days [referred to as the intraseasonal oscillation (ISO; e.g., Madden and Julian 1994), or more commonly known as the Madden–Julian oscillation (MJO)]. The latter variability is manifested as a large-scale eastward-propagating circulation with associated convection anomalies.

Understanding and subsequent prediction of the variability of the tropical atmosphere has been the goal of major international research activities, such as the Tropical Ocean Global Atmosphere (TOGA; World Climate Research Program 1985) and related process experiments [TOGA Coupled Ocean–Atmosphere Response Experiment (COARE); Webster and Lukas 1992]. The importance of the MJO to the goals of these programs and others seeking to extend prediction beyond a few days is well recognized. Many studies have been devoted to documenting the behavior of the MJO, but a detailed understanding of the phenomenon and theories that predict its behavior have been elusive. Consequently, tropical intraseasonal variability has proven difficult to simulate and even more difficult to predict. Slingo et al. (1996), Wu et al. (2002), and Waliser et al. (2003), in comparisons of many models with observations, find marginal evidence of intraseasonal variability. In fact, Krishnamurthy and Shukla (2000) state that ''the intraseasonal component is intrinsically unpredictable. . .'' a point echoed by Sperber et al. (2000) who stated that the overall predictability of the monsoon (i.e., the seasonal average rainfall) ''is likely to be limited by the chaotic, internal variability of the monsoon system.'' The internal variations of the monsoon referred to here include intraseasonal oscillations.

Apparently a more realistic treatment of sea surface temperature (SST) through the use of coupled ocean–atmosphere models (e.g., Inness and Slingo 2003; Inness et al. 2003; Waliser et al. 1999) improves the quality of simulations, albeit in limited ways, and the importance of the coupling between ocean and atmosphere remains a topic of debate. Whereas improvements with coupled models are encouraging, full numerical predictions of monsoon intraseasonal variability, with the skill necessary for useful applications to a user community, appears to be some distance off, although new methods that show promise are now emerging (Webster and Hoyos 2004).

A number of studies, based on analysis of TOGA COARE data in particular, demonstrate a modulation of the SSTs by the MJO (Flatau et al. 1997; Jones et al. 1998; Woolnough et al. 2000; Lau and Sui 1997; among others). These studies, together with improvements exemplified by coupled models, lead to the speculation that the MJO is a coupled mode of the atmosphere–ocean system. However, our knowledge of how the MJO modifies the SST and how the SST variations feed back on the oscillation needs improvement. More recently, studies that embed cloud-resolving models in large-scale atmospheric models reproduce an MJO-like variability without any apparent feedback between convection and SST (e.g., Grabowski 2003; Randall et al. 2003). Thus, debate about the coupled nature of the oscillation remains.

The study reported in this paper further supports the idea that the coupling between the SST and convection in the atmosphere may be an important characteristic of the oscillation. The MJO is characterized in this study in terms of three different data sources, each offering slightly different capabilities and, thus, different insights into the nature of the MJO. TOGA COARE data provide a detailed localized view of the changing nature of convection, surface fluxes, and the SST observed over a period of a few months. Climatological satellite data provide a broader and longer-term perspective of the relation between precipitation, outgoing longwave radiation (OLR) upper-tropospheric humidity, and the SST over a period of several years. The analysis of new data sources derived from the Tropical Rainfall Measuring Mission (TRMM) provide a more intimate view of the relationships between cloud, precipitation, and atmospheric radiative heating. To date, TRMM data have only been compiled for the 1998 calendar year. Analysis of these three data sources provides a consistent picture of the coupling between convection and the atmosphere, creating a form of feedback between the ocean and atmosphere referred to as the humidistat feedback.

The paper begins with a brief description of the data sources used to identify the feedback. Results of the analysis of TOGA COARE data are described in section 3, followed by the introduction of further evidence drawn from climatological sources of satellite data in section 4, including analysis of TRMM data. Section 5 provides a mechanistic picture of a feedback cycle proposed to be an important aspect of the MJO. The feedback concepts derived from the data pull together key processes noted in a number of other studies. For example, the role of solar heating of the oceans under

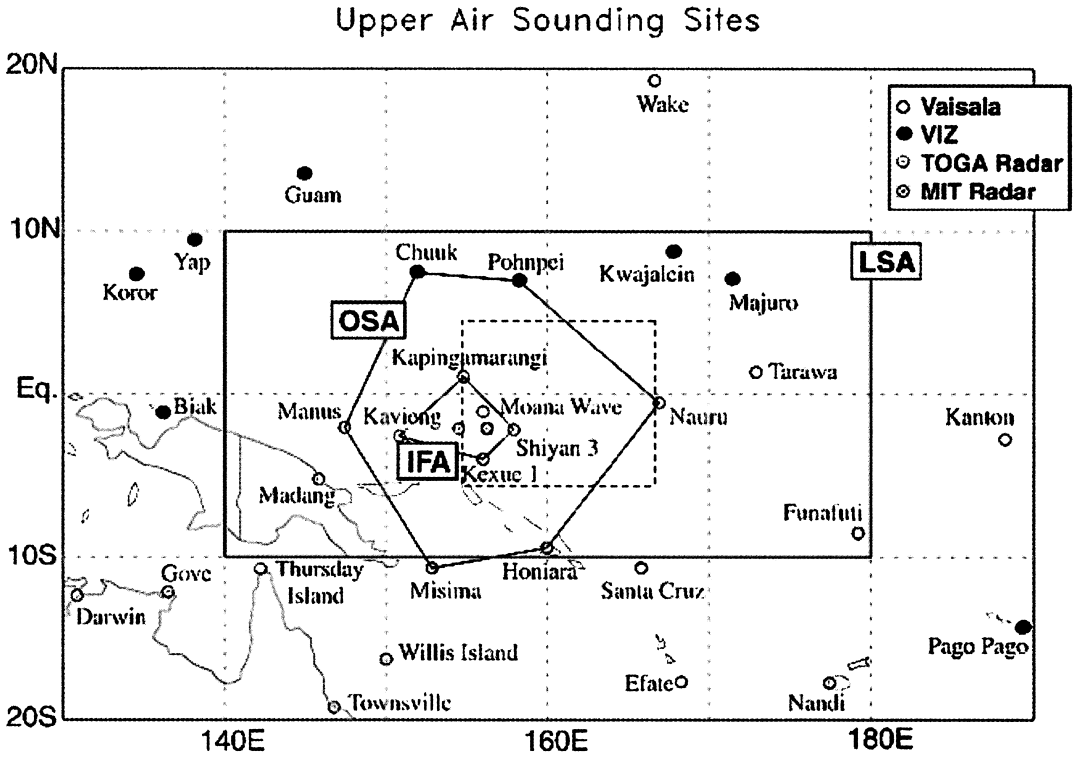

FIG. 1. The region of the TOGA COARE LSA embracing much of the western equatorial Pacific warm pool. Also shown are the TOGA COARE sounding network and the domains of the OSA and IFA. The region denoted by the dashed box is the Fasullo and Webster (1999) region.

clear skies, identified by Waliser and Graham (1993), Flatau et al. (1997), and others is an important aspect of the proposed feedback cycle, as are the radiative destabilization of the clear atmosphere, and the radiative stabilization effects of high clouds (e.g., Lee et al. 2001; Fasullo and Webster 1999) and the SST cooling by increased evaporation associated with convection (e.g., Flatau et al. 1997; Lau and Sui 1997). These processes link producing feedbacks that create a quasi cycle resembling the recharge–discharge concept of Blade and Hartmann (1993). The paper concludes with a summary of its main findings and a discussion of its relevance to the broader issues of climate change.

2. Data sources

a. The TOGA COARE observing network

The TOGA COARE observing strategy and the observing network is described by Webster and Lukas (1992), and a review of the data collected during COARE is provided by Godfrey et al. (1998). In brief, the network consisted of three nested observing arrays designed to study the interactions between the larger-scale circulation of the atmosphere and ocean observed by the large-scale array (LSA) and the smaller, mesoscale circulations associated with convection in the atmosphere resolved by the outer sounding array (OSA) and the intensive flux array (IFA). The domain size and location of these arrays are shown in Fig. 1. The LSA consisted of a network of stations that provided conventional meteorological data from balloonborne sensors (referred to as upper-air soundings) twice daily, and an array of oceanographic moorings. Soundings at sites within the OSA and IFA were conducted 4 times daily. The IFA was centered at 2°S, 156°E and was bounded by a polygon formed by two islands (Kapingamarangi and Kavieng, Papua New Guinea) and two anchored research vessels (*Kexue 1* and *Shiyan 3*). Located within the IFA was the improved meteorological surface mooring (IMET; Weller and Anderson 1996) as shown in Fig. 1. Other research vessels conducted special cruises within the IFA, and a number of research aircraft flights also supplied cloud observations and measurements of other atmospheric properties.

Our analysis ties together TOGA COARE data that have been analyzed individually and described elsewhere. We use the sounding data and budget analyses of Johnson and Cieskelski (2000), together with the surface flux data constructed from observations within the IFA as described in Godfrey et al. (1998). We also augment the TOGA COARE data with the upper-tropospheric (200 hPa) water vapor volume mixing ratio derived from the microwave limb sounder (MLS) flown on the Upper Atmospheric Research Satellite (UARS).

MLS water vapor data are described by Read et al. (1995). The uncertainties are around 20% for the upper tropical troposphere and lower stratosphere.

b. Multisatellite datasets

In addition to the limited-area TOGA COARE data, we analyze other datasets collected over extended periods of time and over the entire tropical oceans in an attempt to demonstrate the more ubiquitous nature and robust features of the feedback. The data include the weekly SST data of Reynolds and Marisco (1993) for the period 1991–95; water vapor radiances of channel 12 of the Television Infrared Observational Satellite (TIROS) Operational Vertical Sounder (TOVS) for the same period, expressed in terms of upper-tropospheric humidity (e.g., Stephens et al. 1996); rainfall estimates from the Global Precipitation Climatology Project (GPCP; Huffman et al. 1997); and OLR from the Advanced Very High Resolution Radiometer (AVHRR; e.g., Gruber and Krueger 1984), flown with the TOVS on the operational polar-orbiting satellites of the National Oceanic and Atmospheric Administration (NOAA). We also use low-level wind speeds derived from radar reflectivity measured by the Active Microwave Instrument on the first *European Research Satellite* (*ERS-1*; e.g., Hsu et al. 1997) averaged weekly for this period.

c. TRMM

The relationship between the radiative heating of the atmospheric column and the evolution of convection and precipitation is a fundamental control of the planetary hydrological cycle (Stephens et al. 1994). Unfortunately, it was not possible to obtain direct estimates of this radiative heating from TOGA COARE data or the above-mentioned satellite data, because radiative fluxes were not measured through the atmospheric column and profile information on clouds was not available to facilitate direct calculation of these fluxes using theoretical models. L'Ecuyer and Stephens (2003) recently outlined an approach for deriving the structure of radiative fluxes in the atmosphere that combines multisensor data from the instruments aboard the TRMM satellite with European Centre for Medium-Range Weather Forecasts (ECMWF) analyses containing assimilated scatterometer winds and clear-sky satellite radiances among other data. The method is also indirect and synthesizes complementary information from retrievals of high cloud optical properties using the Visible and Infrared Scanner (VIRS; Cooper et al. 2003), liquid clouds from the TRMM Microwave Imager (TMI; Greenwald et al. 1993), liquid and ice hydrometeor profiles in precipitation from the TMI-based Goddard Profiling (GPROF) algorithm (Kummerow et al. 2001), and ECMWF analyses to provide input to a broadband radiative transfer model to determine the radiative budget of tropical cloud systems.

Details of the analysis approach and error properties are provided in L'Ecuyer and Stephens (2003). To date TRMM data have only been analyzed for the 12-month period between 1 January 1998 and 31 December 1998. An important difference between this data source and similar data sources is that direct propagation of all uncertainties has been carried out. L'Ecuyer and Stephens (2003) demonstrate that the technique provides monthly mean estimates of oceanic longwave fluxes at 1° resolution to an accuracy of 10 W m^{-2}. Corresponding shortwave flux estimates are found to be accurate to 25 W m^{-2}. Results have also been compared with estimates of outgoing longwave and shortwave radiation at 1.0° resolution from the Clouds and the earth Radiant Energy System (CERES) instrument (Wielicki et al. 1996) observations on a variety of different temporal scales. On short time scales, these differences provide an estimate of the sum of random and bias errors while on longer scales, random errors, by definition, diminish through the averaging process, leaving only the component owing to systematic biases. Uncertainties in instantaneous fluxes are 30 and 77 W m^{-2} in OLR and outgoing shortwave radiation (OSR), respectively. At the other end of the spectrum, the respective uncertainties in long-term means are 8 and 21 W m^{-2}. These results imply that random errors account for between 75% and 85% of the uncertainty in instantaneous fluxes, while the remainder must be due to systematic differences between the two products.

It is important to note that the data invariably suffers errors due to the limited temporal and spatial sampling of the TRMM satellite. While such errors are partially mitigated by compositing methods used, a certain amount of caution is warranted when considering the results. In addition, the analysis period is also strongly influenced by the transition between the strong 1997/98 El Niño and La Niña events. Our analysis of the TRMM data is, thus, limited to the Indian Ocean where there is less influence of El Niño. Figure 2 provides context for the analysis of the data. The diagram presents the OLR derived from AVHRR in the form of a Hovmöller analysis. The OLR is averaged over the latitude band of 5°S–5°N and is shown for longitudes stretching across the Indian and Pacific Oceans. The longitude region noted by the two parallel lines identifies the analysis region of Fasullo and Webster (1999) considered later. In this region we see variability characteristic of the MJO and related changes to SST that do not appear to be adversely affected by the El Niño event.

3. The oscillation of the hydrological cycle and energy fluxes observed during TOGA COARE

a. Hydrological cycle

Figure 3 characterizes the evolution of the state of the warm pool within the IFA for the 4-month duration

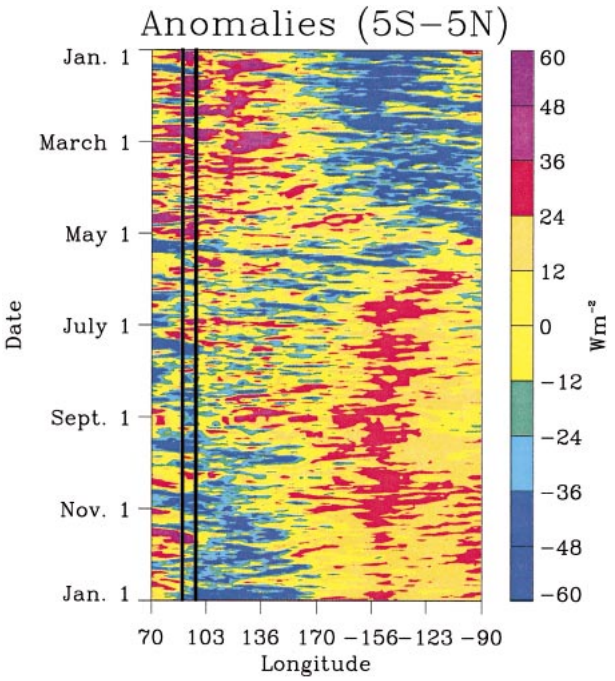

FIG. 2. The time–longitude Hovmöller of AVHRR OLR anomalies for the 1998 calendar year. The anomalies are defined with respect to the 1998 annual mean OLR and are averages between 5°S and 5°N.

of the TOGA COARE intensive observation period (IOP; November 1992 through February 1993). Figure 3a provides the time series of hourly SSTs obtained from the IMET buoy, as well as 24-h SST averages (Weller and Anderson 1996). This time series provides a reference for interpreting other parameters. Two warming–cooling cycles each of approximately 30–60 days duration were observed during the IOP. The maximum SST of this cycle preceded the onset of wide-scale deep convection by slightly more than 1 week (e.g., Nakazawa 1995 and Fig. 3e). The warming phase of the cycle occurred during the latter part of November and into early December when the SSTs reached a maximum in excess of 30°C. This warm phase was followed by a period of marked cooling for the remainder of December into early January. Warming returned and persisted throughout January and into February. Superimposed on this longer-term variation is the striking appearance of the large-amplitude diurnal variations of SST. These variations are most pronounced in the high-insolation, low wind speed phases of the oscillation and are the telltale signatures of these conditions. The large diurnal variation of the surface layer is a critical aspect of the warming of the upper-ocean during this phase (Webster et al. 1996).

A characteristic of the tropical atmosphere important to understanding the variation of SST and the hydrological processes of the MJO are shifts in the wind field that occur on spatial scales of thousands of kilometers

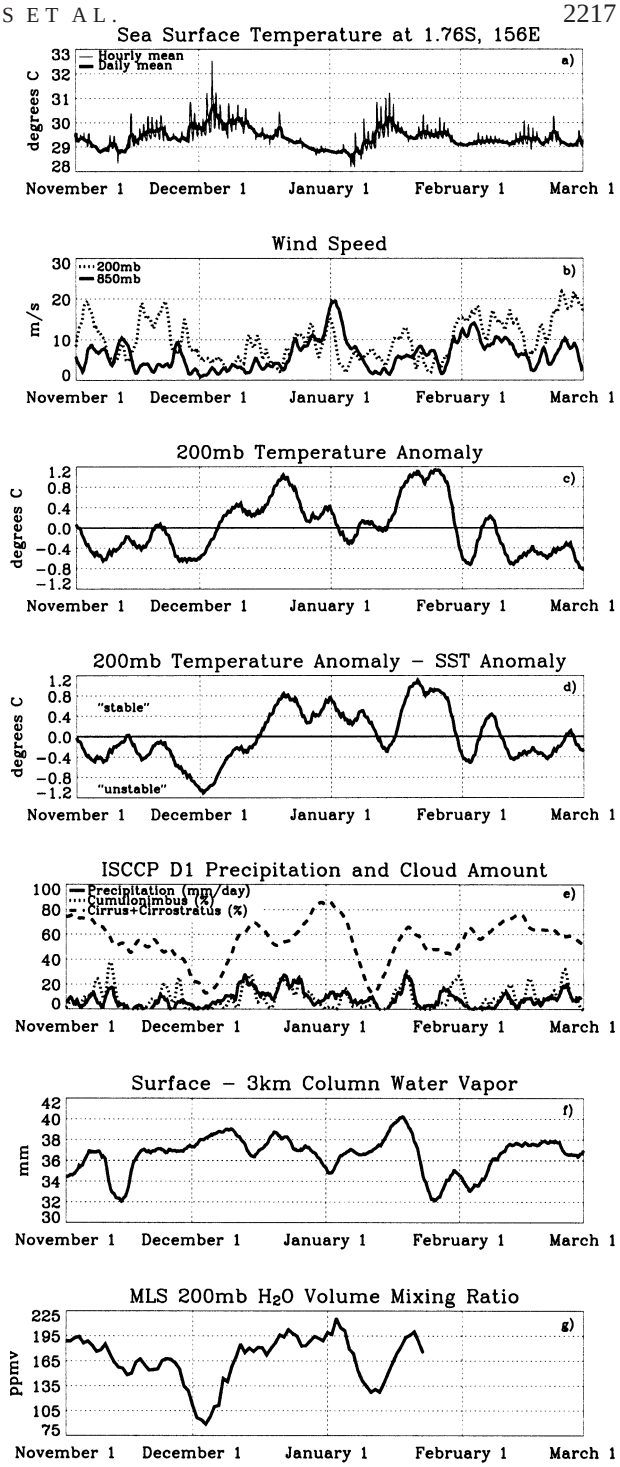

FIG. 3. Time series of (a) hourly and 24-h average SST from IMET; (b) IFA mean 850- and 200-hPa zonal wind speeds (Lin and Johnson 1996); (c) the deviation of the 200-hPa atmospheric temperature from the average during the TOGA COARE period; (d) the difference between the 200-hPa temperature anomaly and the SST anomaly, which acts as a simple proxy of convective instability; (e) average IFA precipitation from budget analysis (Johnson and Ciesielski 1999), the amount of deep convection, and the amounts of high cirrus and cirrostratus over the IFA, as determined by ISCCP, (f) vertically integrated water vapor amount from the surface to 3 km, obtained from the IFA sounding data, and (g) MLS 200-hPa water vapor mixing ratios provided by the MLS flown on UARS.

and last for days to weeks. These are periods of acceleration of the low-level wind and increased easterly wind speeds at higher levels. These changes in the wind field are a large-scale phenomenon referred to as westerly wind bursts (WWBs; Lukas and Lindstrom 1991; Fasullo and Webster 2000). The latter part of December and early January was a notable period of a WWB.

During the TOGA COARE period, the upper-tropospheric temperatures also vary on the time scale of the MJO (Fig. 3c). These temperature fluctuations are reflected in the entire atmospheric column from the surface to the upper troposphere and are consistent with changes in convective available potential energy (CAPE), which conditions the atmosphere for the formation and evolution of organized convection. Figure 3d provides a relative index of atmospheric stability, which may be thought of as a simple way of reflecting the variations on CAPE such that the atmosphere is more stable than average at times when the index is positive and less stable when the index is negative.

Throughout the TOGA COARE period, the mean IFA precipitation (Fig. 3e) closely correlates with the fractional area of the IFA covered by deep convection identified according to a satellite radiance classification scheme developed by the International Satellite Cloud Climatology Project (ISCCP; Rossow and Schiffer 1991). Although precipitation occurred throughout the IOP, including the quiescent periods characterized by SST warming during November, large-scale convection and widespread precipitation followed the maximum SST in early December, leading to a subsequent cooling of the SSTs throughout December.

The evolution of the water vapor (Figs. 3f and 3g) provide conclusive indications of the direct response of upper- and lower-tropospheric water vapor to the cycle of convection. Except for a burst of dry air advected horizontally into the IFA during the middle of November (Yoneyama and Parsons 1999), the lower troposphere generally moistens throughout most of November and into early December. The moistening occurred largely as a result of evaporation of shallow cumulus clouds that develop during that period inferred from observations of the Massachusetts Institute of Technology (MIT) radar aboard the R/V *Vickers* (Johnson et al. 1999). Associated with this moistening is a general drying of the upper troposphere as indicated by the MLS data. This drying is a result of an environment dominated by large-scale subsidence that removes moist air from the upper levels at a rate determined by large-scale radiative cooling (Mapes 2001) and exceeding the moistening of air by evaporation of cloud droplets supplied by the isolated deep convection over the region at that time. The water vapor cycle is reversed with the outbreak of widespread convection that develops over the IFA during December. Water vapor condenses into cloud water, is removed by precipitation falling to the ocean surface, and is lofted by deep clouds to upper levels. The lower levels of the atmosphere dry throughout this stage (Fig. 3f) and the upper troposphere moistens by the sublimation and evaporation of the ice crystals and droplets detrained from the convective systems in the form of widespread upper-level anvil clouds. The MLS water vapor product presented in Fig. 3g is less contaminated by clouds and, thus, not as biased toward clear skies as are other satellite estimates of water vapor (Read et al. 1995 and also Fig. 5 below). The upper-level moistening observed by the MLS sustains high-level clouds over the IFA during the period of convection and after the convection has moved out of the IFA to the east (Fig. 3e).

b. Fluxes and heating rates

A central scientific objective of TOGA COARE was to quantify the heat balance of the upper layers of the western Pacific tropical warm pool which, in part, necessitated the careful calculation of the surface sensible, latent, and radiative heat fluxes. Estimates of the various fluxes have been shown to be within 10 W m^{-2} (Godfrey et al. 1998), allowing for the first time the closing of the upper-ocean heat balance to within narrow bounds.

Figure 4 provides time series of IFA-averaged surface fluxes. The largest observed variations in surface fluxes occurred in both the fluxes of latent heat and solar radiation. The freshening of the low-level winds over the IFA during December produced enhanced evaporation by almost a factor of 3, or about 100 W m^{-2} increases in the fluxes of latent heat. Downwelling solar fluxes, although variable, also decreased locally at the IMET buoy by more than 100 W m^{-2} between late November and late December due to increasing amounts of thick upper-level clouds over the IFA associated with the widespread convection during the period (Fig. 3g). This decrease is also similar in magnitude to that derived from the analysis of TRMM data described below and is similar to the decrease of surface solar irradiance noted by Waliser and Graham (1993).

The integrated radiative heating through the atmospheric column was estimated as a residual term from the heat and moisture budget analysis, given the measured surface sensible and latent heat fluxes, precipitation, and IFA sounding data available from COARE (Johnson and Ciesielski 2000). The variation of this heating (Fig. 4d) has a magnitude of 100 W m^{-2}, which exceeds that reported later from TRMM data (Fig. 6c). This difference is expected given that the data of Fig. 4 are for individual events, and the TRMM results are composites of multiple cases averaged over a larger domain. Nevertheless, the phasing of the variability with respect to the SST variations and high cloudiness is entirely consistent between the two types of data. As we shall see below, the phase of the radiative heating with respect to SST variations is dictated by the variations of high-level cloudiness (Fig. 3e). The relatively clear skies that occur during the height of the SST warming are conditions that lead to more radiant energy emit-

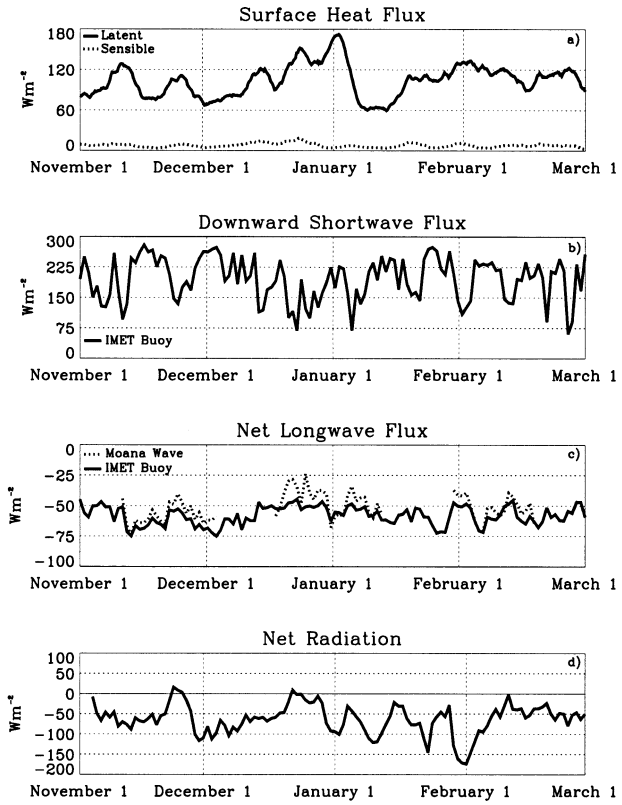

FIG. 4. Time series of (a) the IFA mean surface sensible and latent heat, (b) the incoming daily averaged surface solar radiation, (c) the daily averaged net surface longwave flux, and (d) the net radiative heating of the entire atmospheric column from the surface to the tropopause. All units are W m^{-2}. Sensible and latent heat derived from measurements of four moored buoys in the IFA. Radiative fluxes obtained from the IMET mooring (solid line) and the *Moana Wave* (dashed line). Net heating of the atmospheric column is derived from budget studies using TOGA COARE data (Lin and Johnson 1996; Johnson and Cieskelski 2000).

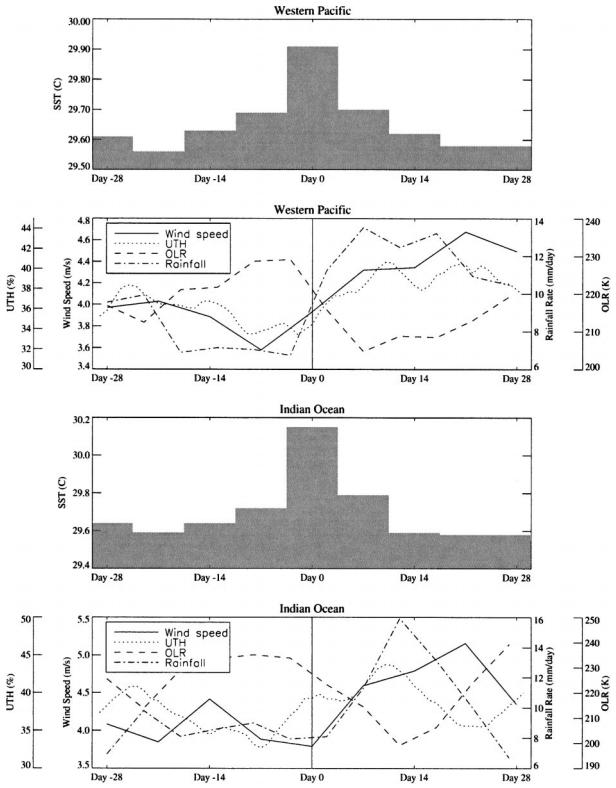

FIG. 5. Composite of the upper-tropospheric relative humidity (UTH), rainfall, OLR, and low-level wind speed (all shown as straight-line curves) expressed relative to the period of the SST cycle (shown as a histogram). The time of maximum SST associated with the latter cycle is indicated as day 0 and all observations are composited relative to that time. Data are shown for a region (top) over the tropical western Pacific between −5°–5°N, and 165°–155°E, and (bottom) over the tropical Indian Ocean between −5°–5°N, and 85°–95°E. The composites represent more than 20 events for each region over the period of 1991–95.

ted from the atmosphere. This is the period of greatest radiation deficit of the atmosphere.

4. Composite satellite data analyses

Although the results shown above apply to the specific region of the IFA of TOGA COARE and specifically for the IOP, we show below that the characteristics of the humidistat feedback extend beyond COARE and, as such, are perhaps a more ubiquitous feature of the tropical atmosphere. The picture that emerges from the composite analyses of the satellite datasets presented here reinforce the view of the oscillation deduced from the TOGA COARE data. The cycles of humidity, wind, precipitation, and radiative heating are obviously connected to the cycle of the SST, suggesting the importance of the coupled nature of the MJO.

a. Climatological analysis

The analysis of the large-scale datasets described above in section 2 are summarized in Figs. 5 and 6. Figure 5 presents the variation of a number of key quantities derived from satellite data as a function of the cycle of SST variation averaged over two large regions of the tropical oceans—one located in the western Pacific that lies within the TOGA COARE region as noted on Fig. 1, and a second region located in the Indian Ocean (refer to the caption of Fig. 5 and Fig. 2 for the domain size and location). The OLR, surface wind, upper-tropospheric water vapor brightness temperatures, and precipitation data are composited relative to warm SST events in the manner introduced by Fasullo and Webster (1999). Warm SST episodes for the two regions are defined by identifying 8-week periods in which the SST exceeded 29.5°C. Day 0 is then that time in this period when the SST is at a maximum. The climatology of these warm events for a 14-yr period from 1982 to 1995 is described in detail by Fasullo and Webster (1999). The climatological variability of SST for the period 1991–95 considered here (and for the 1982–95 period considered in the Fasullo and Webster study) is similar to the variability observed during TOGA

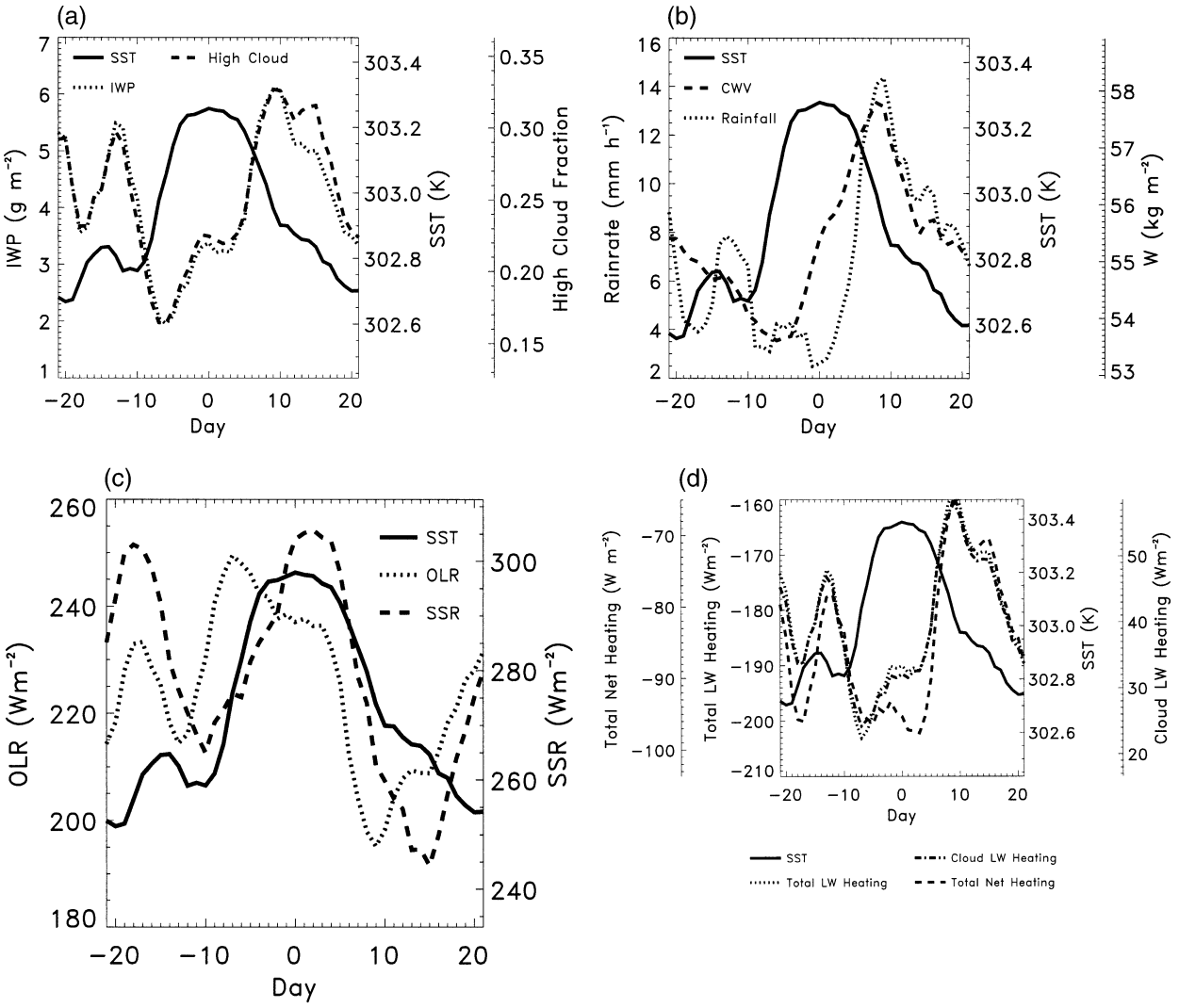

FIG. 6. Composite of TRMM-derived (a) IWP and high cloud fraction; (b) precipitation and CWV; (c) OLR and solar irradiance at the surface; and (d) total column longwave cooling, the net (solar plus longwave) cooling, and the specific contribution to this column cooling by clouds relative to the period of the SST cycle. The time of maximum SST associated with the latter cycle is indicated as day 0, and all observations are composited relative to that time. Data are shown for a region over the tropical Indian Ocean between −5°–5°N, and 85°–95°E.

COARE. The amplitude of this SST variation is smaller due in part to the larger regions considered in this analysis compared the smaller region of the IFA and in part due to the coarseness of the temporal resolution of the SST data used in this analysis.

The variation of SST in relation to the variation of surface wind speeds reveals that the period of SST cooling after day 0 corresponds to a period of marked strengthening of the low-level winds according to *ERS-1* data, similar to that observed during COARE. This period after day 0 is also characterized by increases of the upper-tropospheric humidity preceded by a period of drying of the upper troposphere, also similar to that observed during COARE. The SST cooling phase is also a period of high, cold clouds as indicated by decreased OLR and increased precipitation.

b. TRMM composites analyses

The TRMM data were similarly composited with respect to warm SST events. A number of eastward-propagating convective systems can be identified moving through the Indian Ocean analysis region (delineated by the two solid black lines in Fig. 2). Applying the definition of warm events described above provides four such events over the 1998 analysis period centered around 4 April, 2 May, 16 October, and 28 November, and the composite analysis for these events is presented in Figs. 6a–d.

Figure 6a presents the variation of the cloud ice water path (IWP) and high cloud fraction averaged over the specified region as in Fig. 5 with respect to the phasing of the maximum of the SST. Figure 6b is a similar plot

of the column water vapor and precipitation. The IWP maximum occurs after the SST maximum and coincides with the period of heightened precipitation. Values of the IWP remain elevated, however, beyond the period of significant precipitation by 1 week or more. The column water vapor builds through the latter stages of the warming period of SST and reaches a maximum at the same time of maximum precipitation (almost 10 days after the maximum SSTs) and decreases from that period in a manner consistent with the TOGA COARE data (Fig. 3f).

Figure 6c presents the variability of the top-of-atmosphere (TOA) longwave fluxes (OLR) and the shortwave fluxes. These variations reproduce the behavior already noted with respect to the TOGA COARE data (Fig. 4d) and the satellite data of Fig. 5. The areal mean downwelling shortwave flux at the surface increases through the warming stage due to the clearing skies. This flux then decreases with the cloudiness produced by convection. This areal-averaged decrease is 70 W m^{-2}, as measured from the point of maximum heating near day 0 to the point of minimum solar heating almost 2 weeks later. The latter corresponds to the time of the secondary maximum of IWP. The magnitude of this decrease in solar flux, as already noted, is consistent with the observations over the TOGA COARE IFA and with the flux changes inferred by Waliser and Graham (1993).

Figure 6d presents the the total (longwave plus shortwave) net column radiative cooling (expressed as the column flux divergence), the longwave-only component of this cooling, and the specific contribution by clouds to this column cooling. The scales of these three radiative heating profiles have been adjusted so they overlap one another. Notable features of the results shown are as follows: (i) The characteristics (magnitude and phase) of the variation of the net cooling with SST are broadly similar to the variations of the net radiative heating presented in Fig. 3d. That is, the flux divergence is most negative prior to the period of maximum SST and least negative during and after the deep convection. (ii) The variation in column cooling during this cycle is governed almost entirely by the variation in clouds, which act to reduce the clear-sky column cooling by up to 50 W m^{-2}. (iii) The contribution by clouds to the column cooling is, furthermore, almost entirely through the effects of clouds on longwave absorption and emission. (iv) The variation of column cooling also correlates closely with the variation of IWP and high cloud amount (refer to Fig. 6a) suggesting that it is the upper-tropospheric clouds that govern these cooling variations.

5. Discussion and summary

We now synthesize the observations presented above in an attempt to provide some degree of understanding of the nature of the coupling between the ocean, moist atmospheric thermodynamics, radiation, and the dynamics of the tropical warm pool regions. We propose that these processes establish a feedback that regulates, in unison, the SSTs and hydrological cycle of these regions. This is not to suggest that we consider the MJO to be merely a consequence of thermodynamic/radiative feedbacks, but that these feedbacks interact with and are organized by the dynamics of the MJO in ways that are not yet fully understood.

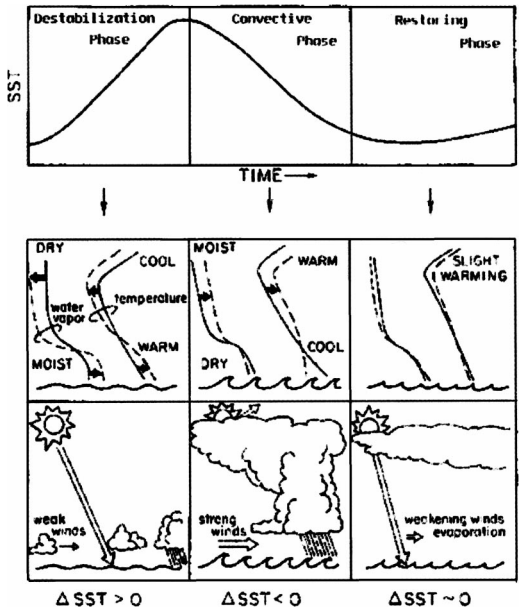

FIG. 7. A schematic of the humidistat feedback showing its three principal phases. (top) The cycle of SST is a simple depiction of the SST variation as a function of time and is used as a reference for defining the three phases of the feedback. (middle) The schematic of how the atmospheric temperature and moisture change during these phases defined with respect to the SST cycle. (bottom) Changes of cloud conditions and associated wind field and heating changes are indicated.

We shall refer to the feedback identified in this paper as the humidistat feedback and argue that it evolves in the three main phases portrayed in Fig. 7. These phases are as follows:

The destabilization phase: This corresponds to a warming phase of SST, such as that which occurred between the later part of November and early December in the TOGA COARE data and is evident in the composite analysis of Figs. 5 and 6 as well as in the time series of Fig. 3. As noted by others, this SST warming phase is induced by quiescent conditions of calm winds resulting in relatively low but nonnegligible evaporation and (near) clear skies. These are conditions that favor strong solar heating exceeding 50 W m^{-2} (Fig. 6b) and weak evaporative cooling of the upper ocean, indicated by the exaggerated diurnal cycle detected by the IMET SST (Fig. 3a). The combination of SST warming and enhanced radiative cooling of the upper atmosphere associated with the lack of high clouds or reduced levels of IWP during this period favors a destabilization of the atmosphere, which can be quantified by a sharp increase of CAPE of the tropical column during these periods

(as implied in Fig. 3d). It is also during this stage that shallow convection begins to increase, resulting in a steady moistening of the low levels, which plays a further role in conditioning the atmosphere for deep convection (Fig. 3f). These conditioning processes do not, however, guarantee the subsequent outbreak of large-scale convection observed during the second phase of the cycle.

The convective phase: The convective phase follows the destabilization stage. The latter is superimposed on a dynamical setting of the MJO that exerts a fundamental control on the triggering of convection and its propagation eastward. The convection that develops is organized into large-scale cloud clusters or supercloud clusters. The convective period is marked by a strengthening of the lower-level winds, a subsequent increase in evaporation from the ocean, and mixing of cold waters upward into the oceanic mixed layer, causing heavy precipitation, a drying of the lower layers of the atmosphere, and a substantial moistening of the upper troposphere. The envelope of deep convection eventually moves out of the region toward the east, proposed to be a manifestation of convectively driven, moist equatorially trapped Kelvin modes (e.g., Gill 1982; Blade and Hartmann 1993). The SSTs cool throughout this period due to a combination of the stronger evaporation, enhanced ocean mixing, and reduced solar heating of the ocean.

The restoring phase: Although there is not a distinct beginning to this phase it occurs with the propagation of the large-scale convective envelope or ''supercluster,'' leaving the IFA filled with high-level clouds associated with the residual moisture. These upper-level clouds, maintained by the residual moisture, reduce the radiative cooling of the atmosphere through absorption of the infrared radiation emitted upward from the warmer atmosphere and surface below (Figs. 4d and 6d). SSTs continue to cool with solar radiation blanketed by these high clouds (Fig. 6c). The combination of SST cooling and the heating of the upper atmosphere by high clouds are major factors that lead to an increase of atmospheric stability and a decrease of CAPE (implied in Fig. 3d) and, together with conditions of strong shear, suppress convection. As the winds weaken and the thick upper-level clouds dissipate to thin cirrus clouds, evaporation from the ocean surface is reduced and solar heating of the upper-ocean mixed layer begins to increase, bringing the cooling of the SSTs to an end and returning to the warming phase with the return of a strong diurnal cycle in the SST (Fig. 3a).

6. Concluding comments

It has been shown that the Madden–Julian oscillation influences short-term weather prediction (Hendon et al. 2000) and it has been speculated that this mode of variability might also project onto El Niño–Southern Oscillation (ENSO; Lau et al. 1989). The present study presents analyses of data from three different sources to suggest the Madden–Julian oscillation is an example of a feedback system in which the hydrological cycle and SSTs mutually regulate one another. The processes that establish this feedback connect clouds and precipitation, radiative transfer, and surface flux exchanges and the SSTs.

These processes are also germane to the broader topic of cloud climate feedbacks. For example, feedbacks involving the radiative heating effects of cirrus clouds and tropical convection and precipitation have also been noted in a number of GCM modeling studies (Slingo and Slingo 1988; Fowler and Randall 1994; Liang and Wang 1997; Ma et al. 1994). The feedbacks between clouds, radiative heating, convection, and precipitation discussed in these studies, and an essential part of the humidistat feedback introduced in this paper, may also be a key to understanding the response of the global hydrological cycle to climate forcing. The broader relevance of the present study to this broader topic follows from the fact that, in the global mean sense, the radiative cooling of the atmosphere is largely balanced by latent heating associated with precipitation. Thus, it is reasonable to propose that perturbations to this radiative cooling, induced in response to carbon dioxide build up, for example, lead to balancing perturbations in latent heating (Stephens 2004, manuscript submitted to *J. Climate*, hereafter STE). The water vapor feedback, for example, increases the column radiative cooling (e.g., Garratt et al. 1999) implying an increase in global precipitation in broad support for the common speculation on an intensification of the hydrological cycle in the era of global warming. The problem with this simple analysis is that a number of other feedback processes come into play to change substantially the cooling of the atmospheric column. Most notable are changes to the amounts of high clouds that significantly alter the atmospheric column radiative heating relative to clear skies (refer to Fig. 6d, e.g.). STE demonstrates that the model-to-model uncertainty in changes to the global precipitation forced by increased carbon dioxide is traceable directly to model-to-model differences in the effects of clouds on the atmospheric radiative cooling.

Because the cloud processes that affect the column radiative cooling are also relevant to the humidistat feedback, it would seem that the MJO might provide a useful paradigm for understanding important aspects of complex cloud–climate feedbacks pertinent for understanding longer-term climate change. Ultimately, the limitation in further advancing our understanding of these feedbacks and their influence on the variability of the hydrology cycle and how it might change in the future is our lack of global observing systems designed to measure not only precipitation but also related hydrological parameters, such as vertical distributions of clouds and the water and ice contents of these clouds, because these properties alter the radiation balance of the atmosphere. This information is expected in the

coming era of the A-Train (Stephens et al. 2002), and advances in understanding the basic connection between radiation and convection can be expected in this coming era.

Acknowledgments. The analysis of the TRMM data was supported under NASA Grant NAG5-11189 Supplement 004. Development of the radiation budget simulator was supported under the U.S. Department of Energy, Office of Science, Office of Biological and Environmental Research, Environmental Sciences Division under Grant DE-FG03-94ER61748 as part of the Atmospheric Radiation Measurement (ARM) Program.

REFERENCES

Blade, I., and D. L. Hartmann, 1993: Tropical intra-seasonal oscillations in a simple non-linear model. *J. Atmos. Sci.,* **50,** 2922–2939.

Cooper, S. J., T. S. L'Ecuyer, and G. L. Stephens, 2003: The impact of explicit cloud boundary information on ice cloud microphysical property retrievals from infrared radiances. *J. Geophys. Res.,* **108,** 4107, doi:10.1029/2002JD002611.

Fasullo, J., and P. J. Webster, 1999: Warm pool SST variability in relation to the surface energy balance. *J. Climate,* **12,** 1292–1305.

——, and ——, 2000: Atmospheric and surface variation during westerly wind bursts in the tropical western Pacific. *Quart. J. Roy. Meteor. Soc.,* **126,** 899–924.

Flatau, M., P. Flatau, P. Phoebus, and P. P. Niiler, 1997: The feedback between equatorial convection and local radiative and evaporative processes: The implications for intraseasonal oscillations. *J. Atmos. Sci.,* **54,** 2373–2386.

Fowler, L., and D. A. Randall, 1994: A global radiative–convective feedback. *Geophys. Res. Lett.,* **21,** 2035–2041.

Garratt, J. R., D. M. O'Brien, G. L. Stephens, M. R. Dix, M. Wild, and J. M. Murphy, 1999: Surface radiation fluxes in transient climate simulations. *Global Planet. Change,* **20,** 33–55.

Gill, A., 1982: *Atmosphere–Ocean Dynamics.* Academic Press, 662 pp.

Godfrey, J. S., R. A. Houze, R. H. Johnson, R. Lukas, J.-L. Redelsperger, A. Sumi, and R. Weller, 1998: Coupled Ocean–Atmosphere Response Experiment (COARE): An interim report. *J. Geophys. Res.,* **103,** 14 395–14 450.

Grabowski, W. W., 2003: MJO-like coherent structures: Sensitivity simulations using the cloud-resolving convection parameterization. *J. Atmos. Sci.,* **60,** 847–864.

Greenwald, T. J., G. L. Stephens, T. H. Vonder Haar, and D. L. Jackson, 1993: A physical retrieval of cloud liquid water over the global oceans using Special Sensor Microwave/Imager (SSM/I) observations. *J. Geophys. Res.,* **98,** 18 471–18 488.

Gruber, A., and A. F. Krueger, 1984: Status of the NOAA outgoing longwave radiation data set. *Bull. Amer. Meteor. Soc.,* **65,** 958–962.

Hendon, H. H., B. Liebmann, M. Newman, and J. D. Glick, 2000: Medium-range forecast errors associated with active episodes of the Madden–Julian oscillation. *Mon. Wea. Rev.,* **128,** 69–86.

Houghton, J. T., L. G. Meira Filho, J. Bruce, H. Lee, B. A. Callandar, E. Haites, N. Harris, and K. Maskell, 1995: *Climate Change 1994: Radiative Forcing of Climate Change and an Evaluation of the IPCC IS92 Emissions Scenarios.* University of Cambridge Press, 339 pp.

Hsu, C. S., T. W. Liu, and M. G. Wurtele, 1997: Impact of scatterometer winds on hydrologic forcing and convective heating through surface divergence. *Mon. Wea. Rev.,* **125,** 1556–1576.

Huffman, G. J., and Coauthors, 1997: The global precipitation climatology project (GPCP) combined precipitation dataset. *Bull. Amer. Meteor. Soc.,* **78,** 5–20.

Inness, P. M., and J. M. Slingo, 2003: Simulation of the Madden–Julian oscillation in a coupled general circulation model. Part I: Comparison with observations and an atmospheric only GCM. *J. Climate,* **16,** 345–364.

——, ——, E. Guilyardi, and J. Cole, 2003: Simulation of the Madden–Julian oscillation in a coupled general circulation model. Part II: The role of the basic state. *J. Climate,* **16,** 365–382.

Johnson, R. H., and P. Ciesielski, 2000: Rainfall and radiative heating rates from TOGA COARE atmospheric budgets. *J. Atmos. Sci.,* **57,** 1497–1514.

——, T. M. Richenbach, S. A. Rutledge, P. E. Ciesiekski, and W. H. Schubert, 1999: Trimodal characteristics of tropical convection. *J. Climate,* **12,** 2397–2418.

Jones, C., D. E. Waliser, and C. Gautier, 1998: The influence of the Madden–Julian oscillation on ocean surface heat fluxes and sea surface temperature. *J. Climate,* **11,** 1057–1072.

Krishnamurthy, V., and J. Shukla, 2000: Intraseasonal and interannual variability of rainfall over India. *J. Climate,* **13,** 4366–4377.

Kummerow, C. D., and Coauthors, 2001: The evolution of the Goddard profiling algorithm (GPROF) for rainfall estimation from passive microwave sensors. *J. Appl. Meteor.,* **40,** 1801–1820.

Lau, K. M., and C.-H. Sui, 1997: Mechanisms of short-term surface temperature regulation: Observations during TOGA COARE. *J. Climate,* **10,** 465–472.

——, L. Peng, C. H. Sui, and T. Nakazawa, 1989: Dynamics of super clusters, westerly wind bursts, 30–60 day oscillations, and ENSO: A unified view. *J. Meteor. Soc. Japan,* **67,** 205–219.

L'Ecuyer, T., and G. L. Stephens, 2003: The tropical oceanic energy budget from the TRMM perspective. Part I: Algorithm and uncertainties. *J. Climate,* **16,** 1967–1985.

Lee, M.-I., I.-S. Kang, J.-K. Kim, and B. Mapes, 2001: Influence of cloud-radiation interaction on simulating tropical oscillation with an atmospheric general circulation model. *J. Geophys. Res.,* **106,** 14 219–14 233.

Liang, X. Z., and W.-C. Wang, 1997: Cloud overlap effects on GCM climate simulations. *J. Geophys. Res.,* **102,** 11 039–11 047.

Lin, X., and R. H. Johnson, 1996: Kinematic and thermodynamic characteristics of the flow over the western Pacific warm pool during TOGA COARE. *J. Atmos. Sci.,* **53,** 695–715.

Lukas, R., and E. J. Lindstrom, 1991: The mixed layer of the western equatorial Pacific Ocean. *J. Geophys. Res.,* **96,** 3343–3357.

Ma, C.-C., C. R. Mechoso, A. Arakawa, and J. D. Farrara, 1994: Sensitivity of a coupled ocean–atmospheric model to physical parameterization. *J. Climate,* **7,** 1883–1896.

Madden, R. A., and P. R. Julian, 1994: Observations of the 40–50 day tropical oscillation—A review. *Mon. Wea. Rev.,* **122,** 814–837.

Mapes, B., 2001: Water's two height scales: The moist adiabat and the radiative troposphere. *Quart. J. Roy. Meteor. Soc.,* **127,** 2353–2366.

Nakazawa, T., 1995: Intra-seasonal oscillations during the TOGA-COARE IOP. *J. Meteor. Soc. Japan,* **73,** 305–319.

Randall, D. A., M. Khairoutdinov, A. Arakawa, and W. Grabowski, 2003: Breaking the cloud parameterization deadlock. *Bull. Amer. Meteor. Soc.,* **84,** 1547–1564.

Read, W. G., J. W. Waters, D. A. Flower, L. Froidevaux, R. F. Jarnot, D. L. Hartmann, R. S. Harwood, and R. B. Rood, 1995: Upper-tropospheric water vapor from UARS MLS. *Bull Amer. Meteor. Soc.,* **76,** 2381–2389.

Reynolds, R. W., and D. C. Marisco, 1993: An improved real-time global sea surface temperature analysis. *J. Climate,* **6,** 114–119.

Rossow, W. B., and R. A. Schiffer, 1991: ISCCP cloud data products. *Bull. Amer. Meteor. Soc.,* **72,** 2–20.

Slingo, A., and J. Slingo, 1988: Response of a general circulation model to cloud longwave radiative forcing. Part I: Introduction and initial experiments. *Quart. J. Roy. Meteor. Soc.,* **114,** 1027–1062.

Slingo, J. M., and Coauthors, 1996: Intraseasonal oscillations in 15

atmospheric general circulation models: Results from an AMIP diagnostic subproject. *Climate Dyn.,* **12,** 325–357.

Sperber, K. R., J. M. Slingo, and H. Annamalai, 2000: Predictability and the relationship between subseasonal and interannual variability during the Asian summer monsoon. *Quart. J. Roy. Meteor. Soc.,* **126,** 2545–2574.

Stephens, G. L., A. Slingo, M. J. Webb, P. J. Minnett, P. H. Daum, L. Kleinmann, I. Wittmeyer, and D. A. Randall, 1994: Observations of the earth's radiation budget in relation to atmospheric hydrology, 4, Atmospheric column radiative cooling over the worlds oceans. *J. Geophys. Res.,* **99,** 18 585–18 604.

——, D. L. Jackson, and I. Wittmeyer, 1996: Global observations of upper-tropospheric water vapor derived from TOVS radiance data. *J. Climate,* **9,** 305–326.

——, and Coauthors, 2002: The CloudSat mission and the A-Train: A new dimension of space-based observations of clouds and precipitation. *Bull. Amer. Meteor., Soc.,* **83,** 1771–1790.

Waliser, D. E., and N. E. Graham, 1993: Convective cloud systems and warm-pool sea surface temperatures: Coupled interactions and self regulation. *J. Geophys. Res.,* **98,** 12 881–12 893.

——, K. M. Lau, and J. H. Kim, 1999: The influence of coupled sea surface temperatures on the Madden–Julian oscillation: A model perturbation experiment. *J. Atmos. Sci.,* **56,** 333–358.

——, and Coauthors, 2003: AGCM simulations of intraseasonal variability associated with the Asian summer monsoon. *Climate Dyn.,* **21,** 423–446.

Webster, P. J., 1994: The role of hydrological processes in ocean–atmosphere interactions. *Rev. Geophys.,* **32,** 427–276.

——, and R. Lukas, 1992: TOGA COARE: The coupled ocean–atmosphere response experiment. *Bull. Amer. Meteor. Soc.,* **73,** 1377–1416.

——, and C. Hoyos, 2004: Predicting monsoon rainfall and river discharge on 15–30 day time scales. *Bull. Amer. Meteor. Soc.,* in press.

——, C. A. Clayson, and J. Curry, 1996: Clouds, radiation, and the diurnal cycle of sea surface temperature in the tropical western Pacific. *J. Climate,* **9,** 1712–1730.

Weller, R. A., and S. P. Anderson, 1996: Surface meteorology and air–sea fluxes in the western Pacific warm pool during the TOGA COARE. *J. Climate,* **9,** 1959–1990.

Wielicki, B. A., B. R. Barkstrom, E. F. Harrison, R. B. Lee III, G. L. Smith, and J. E. Cooper, 1996: Clouds and the earth's Radiant Energy System (CERES): An earth observing system experiment. *Bull. Amer. Meteor. Soc.,* **77,** 853–868.

Woolnough, S. J., J. M. Slingo, and B. J. Hoskins, 2000: The relationship between convection and sea surface temperature on intraseasonal timescales. *J. Climate,* **13,** 2086–2104.

World Climate Research Program, 1995: Scientific plan for the tropical ocean and global atmosphere program. World Meteorological Organization Tech. Document WMO/TD-64, 146 pp.

Wu, M. L. C., A. Schubert, I. S. Kang, and D. Waliser, 2002: Forced and free intraseasonal variability over the South Asian monsoon region simulated by 10 AGCMs. *J. Climate,* **15,** 2862–2880.

Yoneyama, K., and D. B. Parsons, 1999: A proposed mechanism for the intrusion of dry air into the tropical western Pacific region. *J. Atmos. Sci.,* **56,** 1524–1546.